J. Fluid Mech. (2008), *vol.* 609, *pp.* 319–347.
doi:10.1017/S0022112008002292 Printed in the United Kingdom

Dynamics of thin vortex rings

IAN S. SULLIVAN, JOSEPH J. NIEMELA, ROBERT E. HERSHBERGER, DIOGO BOLSTER AND RUSSELL J. DONNELLY

Department of Physics, University of Oregon, Eugene, OR 97403, USA

(Received 2 May 2006 and in revised form 28 April 2008)

As part of a long-range study of vortex rings, their dynamics, interactions with boundaries and with each other, we present the results of experiments on thin core rings generated by a piston gun in water. We characterize the dynamics of these rings by means of the traditional equations for such rings in an inviscid fluid suitably modifying them to be applicable to a viscous fluid. We develop expressions for the radius, core size, circulation and bubble dimensions of these rings. We report the direct measurement of the impulse of a vortex ring by means of a physical pendulum.

1. Introduction

It has been recognized by many investigators that vortex rings are one of the most fundamental and fascinating phenomena in fluid dynamics. Two recent The reviews by Shariff & Leonard (1992) and Lim & Nickels (1995), begin with eloquent discussions of their beauty and utility. We content ourselves here with Philip Saffman's statement, 'one particular motion exemplifies the whole range of problems of vortex motion and is also a commonly known phenomenon, namely the vortex ring ... Their formation is a problem of vortex sheet dynamics, the steady state is a problem of existence, their duration is a problem of stability, and if there are several we have a problem of vortex intractions' (Saffman 1981).

Accordingly, there is also a huge amount of literature on the subject, going back to Reynolds (1876) on the slowing of vortex rings and even earlier to Rogers (1858). Much of this literature involves vortices of substantial core thickness, which is a very difficult problem. The aim of this investigation is to see what can be learned about vortex rings with very thin cores. There is a natural arena for such an investigation: namely the propagation of quantized vortex rings in superfluid helium, where the core has a radius of about 1 Å. The properties and behaviour of quantized vortex rings are thoroughly discussed by Donnelly (1991). An introduction to the problem of core corrections for various models of vortex rings is contained in his § 1.6.

The plan of this paper is as follows. The rest of § 1 is a review of the formulae for thin-core vortices in an inviscid fluid. Section 2 contains the models developed during this study. Section 3 describes the apparatus used in the experiments, which are described in some detail in § 4. Section 5 is a comparison with the work of other investigators.

1.1. *Results for thin-core vortex rings in an invisicid fluid*

Let us first note the results for thin vortex rings of circulation Γ moving in an inviscid fluid of density ρ, quoted in many books on fluid mechanics. When the radius R is much larger than the core radius a, the kinetic energy of such a ring is

Model	α	β
Solid rotating core, constant volume	7/4	1/4
Hollow core, constant volume	2	1/2
Hollow core, constant pressure	3/2	1/2
Hollow core with surface tension	1	0
NLSE solution	1.615	0.615
Viscous core	2.04†	0.558‡

† see (4.6)
‡ Saffman (1970) viscous core

TABLE 1. Values of α and β for classical vortex rings with different core models (adapted from Donnelly 1991). The nonlinear Schrödinger equation (NLSE) result is obtained by Roberts & Grant (1971) for one model of a quantized vortex ring.

(assuming the core is hollow)

$$K = \tfrac{1}{2}\rho\Gamma^2 R\left[\ln\frac{8R}{a} - 2\right]. \tag{1.1}$$

The vortex ring moves forward with its own self-induced velocity V

$$V = \frac{\Gamma}{4\pi R}\left(\ln\frac{8R}{a} - \tfrac{1}{2}\right), \tag{1.2}$$

and the momentum, or more properly impulse, of such a ring is

$$P = \rho\Gamma\pi R^2. \tag{1.3}$$

Thin vortex rings can be described by a total energy (including energy associated with the core structure as well as kinetic energy as in (1.1)) formally equivalent to a Hamiltonian, conventionally denoted as E. Then the velocity and impulse of the vortex rings are connected by Hamilton's equation

$$V = \frac{\partial E}{\partial P}, \tag{1.4}$$

where the details depend on the core model as discussed by Roberts & Donnelly (1970). The simplest situation occurs when the core radius a is negligible in size compared to the radius of the vortex ring. Then the case for any core model can be written

$$E = \tfrac{1}{2}\rho\Gamma^2 R\left(\ln\frac{8R}{a} - \alpha\right), \tag{1.5}$$

$$V = \frac{\Gamma}{4\pi R}\left(\ln\frac{8R}{a} - \beta\right). \tag{1.6}$$

Application of (1.4) to (1.5) using (1.3) gives

$$V = \frac{\partial E}{\partial P} = \frac{\Gamma}{4\pi R}\left(\ln\frac{8R}{a} + 1 - \alpha\right). \tag{1.7}$$

The handling of (1.7) depends on the core structure as shown by Roberts & Donnelly (1970). Thus from (1.6) and (1.7), we see that $\beta = \alpha - 1$ under constant pressure. Under constant volume $\beta = \alpha - 3/2$ (table 1).

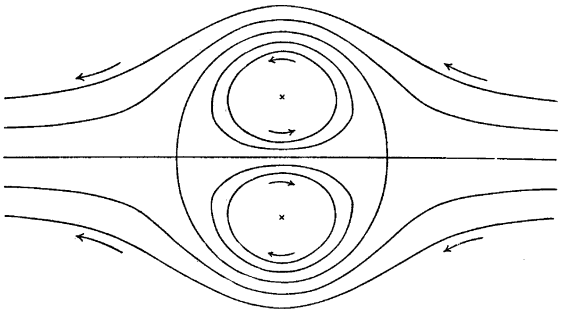

FIGURE 1. A pair of vortex filaments moving through a perfect fluid. (After Lamb 1945).

It is important to note that a direct measurement of the velocity V of quantized vortex rings as a function of energy E was carried out by Rayfield & Reif (1964). Their data allowed the circulation Γ to be measured for the first time, with the result $\Gamma = \kappa \equiv h/m$ where h is Planck's constant and m is the mass of the helium atom. κ is known as the quantum of circulation. This fundamental result assures us that the classical expressions for energy, impulse and velocity for vortex rings in an inviscid fluid, which have been known for decades, have a direct experimental foundation.

1.2. *Fraenkel's second-order formulae*

Fraenkel (1972) has given second-order formulae for rings which have finite, but small values of $\varepsilon = a/R$, the dimensionless core radius. These are written

$$P = \rho\Gamma\pi R^2\left(1 + \tfrac{3}{4}\varepsilon^2\right), \tag{1.8}$$

$$E = \tfrac{1}{2}\rho R\Gamma^2\left[\ln\frac{8}{\varepsilon} - \frac{7}{4} + \frac{3}{16}\varepsilon^2\ln\frac{8}{\varepsilon}\right]. \tag{1.9}$$

Since ε is considered small in this paper, we see $\alpha = 7/4$ in (1.5).

1.3. *Velocity of a vortex ring in a viscous fluid*

Equation (1.6) is the celebrated relationship between V, R, Γ and a for vortex rings in an inviscid fluid. Before proceeding too far in new investigations, we would like to know if a similar expression exists for vortex motion in a viscous fluid. Indeed such an expression as (1.6) has been introduced by Saffman (1970) for a Gaussian vorticity distribution in the core: it is identical to (1.6), which we will discuss in § 4.3 below, and where he finds

$$a = \sqrt{4\nu T}, \quad \beta = 0.558, \tag{1.10}$$

where ν is the kinematic viscosity and T is the stroke time for the piston. This result holds only for small times. If the time of observation is limited to the moment of formation we will show that (1.6) and (1.10) give a good account of experiments reported here. There are some problems for $t > T$, which we will discuss in § 4.4.

1.4. *The vortex bubble*

We can gain some insight into the vortex bubble from a drawing in Lamb (1945, p. 155), reproduced here as figure 1. This represents two infinitely thin straight vortices with cores situated at $+R$ and $-R$, moving through the fluid at velocity $\Gamma/4\pi R$, where Γ is the circulation about the filaments. The picture is drawn from a frame at rest with respect to the vortex filaments. The oval surrounding the vortices moves with the vortex pair. The semi-axes of the oval are $2.09R$ and $1.73R$, and the ratio of semi-minor to semi-major axes is $\gamma = 0.828$.

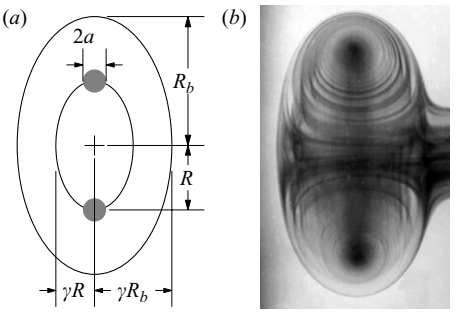

FIGURE 2. (*a*) Sketch of a thin vortex ring of core radius a, ring radius R and bubble radius R_b. γ is the ratio of semi-minor to semi-major axes. The direction of motion is horizontal. Streamlines would look much as in figure 1. (*b*) Photograph of a ring that has just passed through a sheet of tracer, which casues the apparent jet on the right. The comparison with (*a*) is clear.

We can understand the presence of the vortex bubble by a simple analogy from electromagnetism. Suppose we have a current loop carrying a current density j in an external magnetic field B. The current loop generates a dipolar magnetic field of its own which 'overrides' the external field near the loop. There is a well-defined spherical boundary within which the field from the loop dominates and outside of which the external field dominates (we can picture the analogy by considering figure 1 to have a current loop instead of parallel wires). The current density j is analogous to the vorticity in the core, and B is analogous to fluid velocity V (see Fetter & Donnelly 1966). Clearly, the vortex bubble disappears if the ring stops moving, just as the spherical boundary vanishes if B is made to vanish.

Beginning with these concepts, we aim to find expressions for the various quantities described in § 1.1 which are related to the parameters of the gun: stroke length L, stroke time T and gun radius R_0.

2. Models

2.1. *The radius of vortex rings*

We would like to characterize our rings in water by means of equations along the lines of those discussed in § 1.1. We have devised a way of measuring the core size a and impulse P directly, and will describe these methods and determinations below.

In this study, vortex rings are generated by impulsively displacing water with a piston through a cylindrical gun, the details of which are described in § 3. When the piston is fired, it sweeps out a volume of fluid $\Omega_p = \pi R_0^2 L$. The fluid associated with the vortex ring and its flow pattern form a vortex bubble, which is flattened in the direction of propagation of the ring as (figure 2). Let us assume it is an ellipsoid of revolution with semi-major axis R_b and semi-minor axis $\gamma R_b$where the eccentricity $\gamma < 1$. The volume of this spheroid would then be $\Omega_b = (4\pi/3)R_b^3\gamma$. Measurements show that the volume of this bubble is greater than Ω_p owing to entrainment of surrounding fluid during the formation process as described by Dabiri & Gharib (2004).

We make use of these ideas in the calculations of ring and bubble dimensions. Assuming that the impulse of the ring P defined in (1.3) is approximately equal to the momentum given to the water by the piston (a fact later verified experimentally

in § 4.5) we have

$$M_p V_p = \rho \Gamma \pi R^2, \tag{2.1}$$

where M_p is the mass of water displayed by the piston and $V_p = L/T$ is the velocity of the piston. At the same time, when the ring is moving with its bubble at velocity V,

$$M_p V_p = M_b V, \tag{2.2}$$

where V is the velocity of the vortex ring and M_b is the mass of fluid in the ring–bubble complex. The practical use of (2.2) requires an amendment to include the induced mass of the bubble, as will be explained below.

We have found it useful to imagine that the vortex ring itself encircles the major axis of an entirely fictitious and geometrically similar ellipsoid, as indicated by the inner curve of figure 2(*a*). The volume of fluid in the inner spheroid is $\Omega_r = (4\pi/3)R^3\gamma$, and if we guess that its volume is equal to the volume swept out by the piston, Ω_p, then

$$\Omega_r = \Omega_p \tag{2.3}$$

and

$$R = \left(\frac{3\Omega_p}{4\pi\gamma}\right)^{1/3} = \left(\frac{3R_0^2 L}{4\gamma}\right)^{1/3}. \tag{2.4}$$

The assumption (2.3) is unlikely to be exact, but is justified *a posteriori* by the good correlation of figure 5 in § 4.

2.2. *An estimate for vortex circulation and velocity*

What would help the designer of an experiment is an estimate of the expected ring circulation based on the stroke length and stroke time. Here we appeal to a simple argument called the 'slug model' (see, for example, Didden 1979). This model assumes that the ring is formed from a cylindrical 'slug' of fluid with U_0 the velocity at the exit of the tube at the axis of symmetry which is ejected from the nozzle. The slug model is based on the flux of vorticity from the nozzle. The result is an expression for the circulation

$$\Gamma_s = \frac{L^2}{2T}, \tag{2.5}$$

assuming the stroke length is L and the stroke time is T. In this expression, we use the original slug model and have neglected the overpressure correction term (which is necessary for the formation of the vortex ring), (Krueger 2005). Using (2.4) for the ring radius then the expected velocity of the rings at the gun based on the slug model of circulation is

$$V_s = \frac{\Gamma_s}{4\pi R}\left(\ln\frac{8R}{a} - \beta\right) = \frac{L^2}{8\pi R T}\left(\ln\frac{8R}{a} - \beta\right), \tag{2.6}$$

This observation leads us to attempt another estimate of the circulation based upon the assumption that the impulse of the ring is not far from the momentum given to the water in the gun by the piston, later verified experimentally in § 4.5. Thus from (2.1),

$$\rho\pi R_0^2 L V_p = \rho \Gamma \pi R^2, \tag{2.7}$$

we have an expression for the circulation in terms of gun parameters

$$\Gamma = \frac{R_0^2 L V_P}{R^2} = \frac{R_0^2 L^2}{R^2 T}, \tag{2.8}$$

and the corresponding velocity V using (1.6), (1.10) and (2.4) is

$$V = \frac{\Gamma}{4\pi R}\left(\ln\frac{8R}{a} - 0.558\right) = \frac{\gamma V_p}{3\pi}\Lambda, \tag{2.9}$$

where

$$\Lambda = \ln\frac{8R}{a} - 0.558. \tag{2.10}$$

2.3. *The core size*

There is a remarkable prediction of the propagation velocity of a vortex ring in a viscous fluid by Saffman (1970). Saffman supposed that the vorticity in the core of the vortex ring has a Gaussian distribution given by

$$\omega_\phi = \frac{\Gamma}{4\pi\nu t}\left\{\exp\left(\frac{-r^2}{4\nu t}\right)\right\}, \tag{2.11}$$

where t is measured from a virtual origin where the core is of zero diameter. He then derived the propagation velocity to leading order

$$V = \frac{\Gamma}{4\pi R}\left\{\ln\frac{8R}{\sqrt{4\nu t}} - 0.558\right\}, \tag{2.12}$$

valid for small times where the core remains small. Comparing (2.12) with (1.6) suggests a guess for the core parameter:

$$a = \sqrt{4\nu T}, \tag{2.13}$$

where $t = T$ is the stroke time of the gun. This result is verified experimentally in § 4.3. Furthermore, the value of β discussed in table 1 is clearly 0.558.

2.4. *Dimensions of the vortex bubble in water*

Equation (2.9) shows that the velocity of the ring–bubble complex is directly proportional to the velocity of the piston, $V_p = L/T$, so conservation of momentum allows us to solve for the mass and hence the volume of the bubble (including the fluid within the ring). From (2.2), we obtain

$$M_p V_p = \rho\Omega_p V_p = \rho\pi R_0^2 L V_p = M_b V. \tag{2.14}$$

The volume of the bubble is

$$\Omega_b = \frac{4}{3}\pi R_b^3\gamma \tag{2.15}$$

and its momentum in flight is $M_b V$. However, as observed by Baird, Wairegi & Loo (1977), the creation of the bubble by the piston involves the induced (or added) mass M_i. The mass of the bubble in the momentum balance relation (2.14) which we call M_b' must include the induced mass M_i which is usually written $M_i = k\rho\Omega_b$. For a sphere $k = 1/2$. For more general shapes, we can refer to § 80 of Loitsyanskii (1966). The case shown in figure 2(*b*) has $\gamma \simeq 0.6$, $k = 0.65$. Thus the momentum balance in (2.2) is amended to read

$$M_p V_p = M_b' V, \tag{2.16}$$

where $M_b' \simeq M_b + kM_b = (1+k)M_b$. Therefore the mass of the bubble associated with the ring is given by $M_b = M_p V_p/(1+k)V$ and the corresponding radius is

$$R_b = \left[\frac{9\pi R_0^2 L}{4\gamma^2\Lambda(1+k)}\right]^{1/3}, \tag{2.17}$$

which using (2.4) leads to

$$\frac{R}{R_b} = \left[\gamma(1+k)\frac{\Lambda}{3\pi}\right]^{1/3}, \tag{2.18}$$

independent of R_0, L and only logarithmically dependent upon T.

We define the entrained fluid fraction $\eta = (\Omega_b - \Omega_p)/\Omega_b$, which in our experiments is given by,

$$\eta = 1 - \frac{\Lambda(1+k)\gamma}{3\pi}, \tag{2.19}$$

again independent of R_0, L and only logarithmically dependent upon T.

2.5. *The slowing of vortex rings*

There are a number of reasons why vortex rings might slow down. One common suggestion is that the core grows by diffusion, reducing the velocity by (1.6), another that bending waves grow and take energy from the ring, or that the ring may become turbulent in some sense and start to break up. Reynolds (1876) observed that 'rings grow in size as they proceed, and consequently they are continually adding to their bulk water taken up from that which surrounds them, and with which this forward momentum has to be shared. A loss of velocity must result from this growth in size.'

One of the commonly cited works that discusses the slowing of vortex rings is Maxworthy (1972). He states that the velocity decays exponentially with the distance travelled by the ring and is proportional to $1/t$ for long times. Maxworthy observes that there is viscous entrainment of the fluid surrounding the vortex bubble as well as a detrainment of rotational fluid ejected into a wake that trails the ring, a combination of which results in the slowing of the vortex ring. This phenomenon of entrainment and detrainment was first observed by Krutzsch (1939). He fired vortex rings through sheets of dyed fluid, which initially wrapped up around the bubble and were then shed into the wake of the ring.

Since the rings in the present study have quite small cores, and do not change their radius during propagation, it is tempting to consider viscous drag on the core, much as was done in experiments in superfluid helium. The role of friction on quantized ring vortices has been reviewed by Barenghi, Donnelly & Vinen (1983). They compute the drag per unit length on the core, and since the circulation is quantized, the only way to lose energy is to reduce the radius of the ring (recall the energy of a vortex ring is proportional to its radius as in (1.5). This shrinking actually causes the ring to travel faster, as we see from (1.6), and we have the unusual situation that quantized vortex rings speed up as they decay. We therefore proceed to model the viscous drag on the core in the spirit of the liquid helium investigators. It is important to note that with this 'drag' concept we aim to capture all the physical mechanisms that slow the ring down.

Of course we do not know the relevant drag coefficient for anything as exotic as a viscous vortex core (such as that suggested by Saffman), but we can certainly try to measure it. Let us define the drag coefficient on the core as

$$C_{dc} = \frac{D_f}{\frac{1}{2}\rho V^2 A}, \tag{2.20}$$

where V is the ring velocity and $A = 2a \times 2\pi R$, where, as usual, $a \ll R$. The drag force will result in a loss of impulse given by

$$D_f = C_{dc} \times \tfrac{1}{2}\rho V^2 \times 4\pi a R = -\frac{\mathrm{d}P}{\mathrm{d}t}, \tag{2.21}$$

where P is given by (1.3). Thus the circulation decreases according to

$$\frac{\mathrm{d}\Gamma}{\mathrm{d}t} = \frac{4\pi R}{\Lambda}\frac{\mathrm{d}V}{\mathrm{d}t}, \tag{2.22}$$

where Λ is given by (2.10).

If X is the distance travelled from the gun and V_0 is the speed at the mouth of the gun as given by (2.9), then the velocity at distance X is

$$V = V_0 \mathrm{e}^{-cX} \tag{2.23}$$

and the velocity at time t is

$$V = \frac{V_0}{1 + V_0 ct}, \tag{2.24}$$

where the damping coeffient c is

$$c = \frac{C_{dc} a \Lambda}{2\pi R^2}. \tag{2.25}$$

It is worth noting that the velocity decays exponentially with distance and as $1/t$ for large times, which is in agreement with the predictions of Maxworthy (1972) and the experiments of Scase & Dalziel (2006). The distance $X(t)$ travelled by time t can be written

$$X(t) = \frac{1}{c}\ln\left(V_0 ct + 1\right), \tag{2.26}$$

and (2.26) can be directly compared to experiment.

Note that we could calculate the drag on the vortex bubble instead of the vortex core and achieve the same equations with modified drag coefficients. Since the damping coefficient c defined in (2.25) remains the same, it is easy to convert one drag coefficient to another.

It is well known that a circular vortex ring has a translational velocity which arises from its own curvature (the smaller the radius R of the ring, the faster the ring travels). More quantitative knowledge is now available about the slowing of a ring vortex by finite-amplitude Kelvin waves. Building on a seminal paper by Kiknadze & Mamaladze (2002), Barenghi, Hänninen & Tsubota (2006) using the exact Biot-Savart Law, have analysed the motion of a vortex ring in an inviscid fluid perturbed by Kelvin waves of finite amplitude. They have found that the translational velocity of the perturbed ring decreases with increasing amplitude; at some critical amplitude, the velocity becomes zero, that is, the vortex ring hovers like a helicopter. A further increase of the amplitude changes the sign of the translational velocity, that is, the vortex ring moves backward. This remarkable effect is due to the tilt of the plane of the Kelvin waves which induce motion in the 'wrong' direction. The magnitude of the tilt oscillates, what results is a wobbly translational motion in the backward direction. They have also found that the frequency of the Kelvin wave decreases with increasing amplitude and that the total length of the perturbed vortex ring oscillates with time. This oscillation in vortex length is related to the oscillation of the tilt angle. This analysis suggests that the velocity of vortex rings may well depend on the amplitude of Kelvin waves at the time of formation. Rings with substantial amplitude of Kelvin waves will be expected to move more slowly than rings with little or no Kelvin wave amplitude. Thus, we may expect different investigators to observe different ring velocities under nominally identical values of L and T. Indeed, successive rings from the same gun could well have Kelvin waves of different phase and

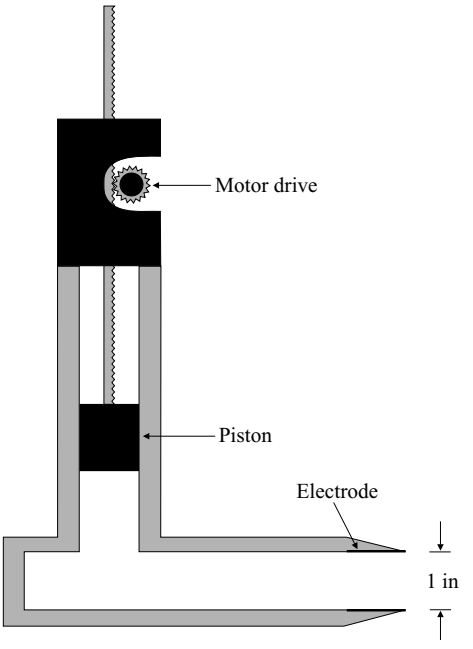

FIGURE 3. The vortex gun used for most of the experiments reported here.

different amplitudes. This may well explain the large scatter we often see in vortex-ring experiments.

3. Apparatus

3.1. *The vortex guns*

3.1.1. *The orginal vortex-ring gun*

The vortex guns shown in figures 3 and 4 have an exit diameter of $D_0 = 2.54$ cm. Embedded in the wall at the exit is the cathode for the Baker visualization technique. A rod suspended elsewhere in the tank serves as the anode.

A small servo motor mounted on the gun assembly shown in figure 3 drives the rack via a pinion gear. The servo motor incorporates an encoder to provide positional feedback. The gun is capable of a stroke length limited to between about 1 and 4 cm. Less than 1 cm is unusable owing to mechanical backlash.

The servo motor is driven by a custom built servo amplifier The amplifier maintains the position of the motor based upon a command voltage level input. The amplifier incorporates two linear feedback loops – a proportional loop and an integral loop. The proportional loop generates a motor drive based upon the positional error signal. The integral loop generates a motor drive based upon the time integral of the error signal.

One of the analogue voltage outputs from a National Instruments PCI-MIO-16XE-10 card is connected to the command input of the servo amplifier. A custom program written in National Instruments LabView Version 5.0 is used to generate the trajectory profile for the motor. Usually a constant-velocity ramp (based upon the L and T variables) is used to generate the rings. This gun design has been shown to be capable of generating rings as fast as 40 cm s^{-1}. The performance of the gun has not been entirely satisfactory, however, owing to the problems of aligning the rack and pinion and piston, and to vibrations transmitted to the tank.

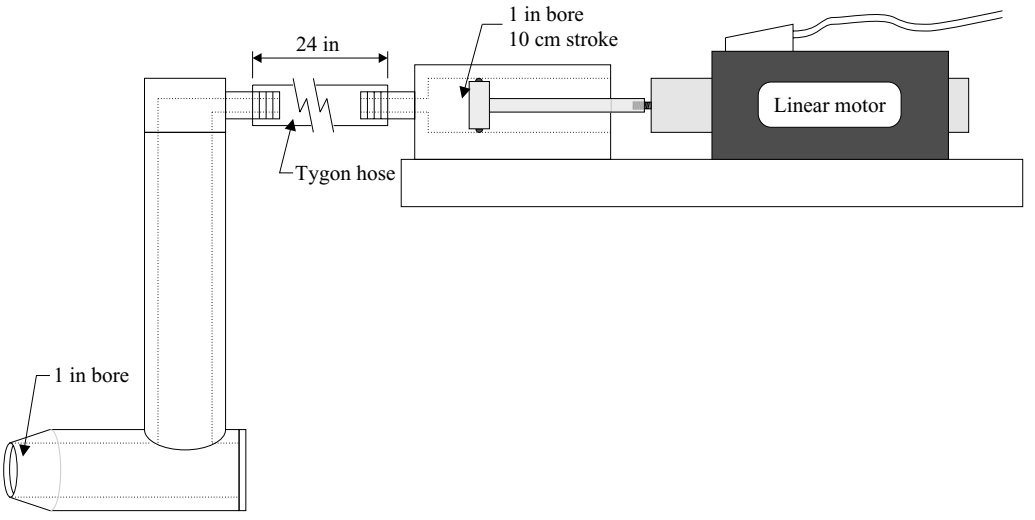

FIGURE 4. An improved vortex gun used only recently. Brushless/ironless; 1.74 kg thrust rod; 780 N maximum thrust; 12 μm resolution.

3.1.2. *The new vortex-ring gun*

The newer gun shown in figure 4 has the same electrodes as the older gun. The new gun is now constructed in two separate parts. The guns are hollow 1 in diameter tubes, bent at 90°. Separate 1 in diameter cylinder and piston assemblies are connected to the gun via plastic tubing. The tubing must be reinforced so that it does not expand during the piston stroke. Twin O-ring seals provide the pistons with a water-tight fit to the cylinders. The pistons are driven by Copley model STA2510S-104-S-S03X linear motors (capable of 780 N of peak thrust). The pistons are directly attached to the magnet rods of the motors, eliminating mechanical backlash. Also, the motors are brushless and ironless, resulting in smoother motion due to minimal motor cogging. The motor and piston assemblies provide a stroke length anywhere between 0 and 10 cm.

The motors are driven by a Copley model XSL-230-18 Xenus indexer/amplifiers. Since the motors are brushless, electronic commutation is provided by the Xenus amplifiers via linear Hall-effect sensors mounted on the forcer assembly. These same sensors also provide positional feedback. The basic resolution of the motors is 12.5 μm. The Xenus amplifiers are an entirely digital system, allowing ready reprogramming of the feedback-loop coefficients, and they also internally generate the motion trajectory based upon variables sent via an RS-232 link.

Our piston velocity follows a trapezoidal ramp. Setting the piston velocity at 32 cm s^{-1}, the rise time from rest to 32 cm s^{-1} was 0.025256 s and the fall time was 0.028392 s. Thus the average acceleration is 1267 cm s^{-2} and the average deceleration was 1127 cm s^{-2}.

Based upon preliminary usage, the new gun provides smooth repeatable performance and beautiful consistent rings. The piston can reach 50 cm s^{-1}. With optimization of the feedback loops, even better performance may be possible.

3.2. *Visualization technique*

We use the Baker (1966) technique for visualization of fluid flows. It consists of generating hydroxyl ions (OH^-) *in situ* in a flowing fluid by electrochemical means.

An acid–base indicator is added to the solution, which has been adjusted to an appropriate pH. The local generation of hydroxylions will change the pH locally and hence the colour of the indicator will change locally. One immediate advantage of this technique is that the tracer is neutrally buoyant. It can work in stratified flows; it is also free from influence by centrifugal forces, and hence is useful in rotating experiments. It works even in glycerol–water mixtures. This technique is useful also because the voltage and the length of time it is applied can be computer controlled.

The working fluid is prepared by adding enough thymol blue indicator to 1000 ml of distilled water to produce a 0.01 % solution by weight. This solution is titrated to the endpoint (pH $\simeq$ 8.0) by adding 1 N sodium hydroxide (NaOH) drop ($\approx 0.25\,\mathrm{cm}^3$) drop by drop until it turns deep blue, then adding one drop of 1 N hydrochloric acid (HCl) to cause the solution to be on the acid (or yellow) side of the endpoint. Although Baker does not suggest this, a small amount of NaCl was occasionally added to increase the conductivity of the solution in the experiments described below. Of course, the preparation of the system as just described self-generates some sodium chloride (NaCl) in the solution.

As the fluid flows, the hydroxyl ions are carried along as part of the moving fluid particles. (The word particle is used here in the fluid dynamics sense, and not in the sense of atom or molecule.) Hence the colour moves with the flowing fluid. It is important to realize, however, that the colour tags the fluid particles that have a certain pH, not the velocity in its own right. If the particle is moving, the colour motion will show how, but if the fluid particle is stagnant, the colour will persist as long as no process changes the pH. Typically, 8 V was sufficient to give good visualization in a short time. However, any voltage above about 2 V will produce electrolysis of water and produce hydrogen bubbles, which by themselves gave some useful visualization of vortex rings, as the bubbles are attracted to the vortex core by the pressure gradient, just as ions are attracted to quantized vortex cores for quantized vortices in helium II. However, trapped hydrogen bubbles in sufficient quantity could alter the dynamics of the vortex rings in unknown ways, and even cause them to become buoyant. As a result, we have come to use about 2 V, and wait longer for the 'ink' to appear. This technique is particularly useful because the voltage can be computer controlled, and, as we shall see below, it also works for glycerol–water solutions, so that the viscosity can be customized to a given experiment.

There is no doubt that the Baker technique is useful for flow patterns such as steady or oscillating Taylor vortex flows (see Park, Barenghi & Donnelly 1980; Hollerbach *et al.* 2002). As far as we can ascertain, the tracer follows the fluid motion faithfully, except when the motion ceases; then ionic recombination sets the time scale for disappearance of the tracer (perhaps a few minutes). Note that the oscillating Taylor vortex flows cited above have diffusion of vorticity which is marked because the electric field generates hydroxyl ions continuously at the anode. If the electric field is absent, the hydroxyl ions have low diffusivity and will not follow diffusion of vorticity (i.e. there is a high Schmidt number, of order 6000). This is of considerable interest to our vortex rings, because they detach from the anode on formation, and the 'ink' then has a very high Schmidt number.

A thorough discussion of the Baker technique is contained in Mazo, Hershberger & Donnelly (2008).

We also used Kalliroscope AQ-1000 to study vortex rings in water. Kalliroscope is a commercial product first described scientifically in a paper by Matisse & Gorman (1984). Exactly what is shown by light reflection from these anisotropic particles is still not entirely clear, although an analytical study by Savas (1985) suggests that the flakes

		R (cm) at	
L (cm)	T (s)	5 cm	28 cm
2.0	0.07	1.44	1.46
2.5	0.07	1.51	1.49
3.0	0.07	1.58	1.58
3.5	0.07	1.62	1.63
4.0	0.07	1.64	1.60

TABLE 2. Comparison of the radii of several rings at 5 and 28 cm from the gun.

align themselves with stream surfaces with rapid turnovers and further notes that it is a useful technique for determining certain flow patterns. A discussion by Gauthier, Gondoret & Rabaud (1998) is useful in this respect: in particular, they show that the observed light cannot be used to reconstruct the velocity field. However, they do show that Kalliroscope can be used specifically to visualize a vortex core in Taylor–Couette flow by comparing numerical predictions to experimental observations. Much qualitative information has been obtained about vorticity patterns in Taylor–Couette flow.

The contrast between the two visualization techniques is important to note. In the Baker technique the marker tracks fluid particles; Kalliroscope can be thought of roughly as marking regions of concentrated vorticity.

4. Experimental results

We study some of the basics of vortex rings in water with a few preliminary experiments. We observe that the rings have thin cores, as would be expected from the relative smallness of the stroke. The dimensionless ratio of stroke length L to orifice diameter D_0, L/D_0, is called the 'formation time' and in our experiments is generally less than 2. Here, $D_0 = 2R_0$. Gharib, Rambod & Shariff (1998) show that for $L/D_0 < 4$, only an isolated ring is formed, whereas for $L/D_0 > 4$, the flow field consists of a vortex ring followed by a trailing jet. The diameter of the rings, $2R$, is approximately the same as the exit diameter D_0, and is found to increase slowly with the stroke length L and is independent of stroke time T. In our experiments, the diameter of the rings was measured photographically with a high resolution digital camera. The rings can move quickly, spanning a velocity range from about $1\ \mathrm{cm\,s^{-1}}$up to about $50\ \mathrm{cm\,s^{-1}}$. The diameter of the rings appears to remain constant during propagation, and eventually rings exhibit bending waves on the cores. In what follows, it is important to realize that we are discussing the motion of vortex rings in a viscous fluid in the limits $a/R = 0$ and $L/D_0 = 0$ (except if L/D is too small the vortex may move back into the gun).

The Reynolds numbers can be variously defined. Unless otherwise mentioned, we take $Re \equiv \Gamma/\nu \simeq 100\Gamma$ appropriate to experiments in room temperature water.

4.1. *The radius of vortex rings and of the bubble*

The ring radius as given by (2.4) does not involve space or time and hence we do not expect the radius to change by much as it propagates across the tank. Data supporting this is given in table 2 where we compare ring radii at 5 cm and 28 cm from the gun. The results in table 2 show that we may take the ring radius to be constant while slowing down to very good accuracy. Equation (2.17) suggests that except for

t (s)	R_b (cm)
1	3.4
4	3.4
8	3.6
12	3.4

TABLE 3. Measurements of the bubble radius as a function of flight time t.

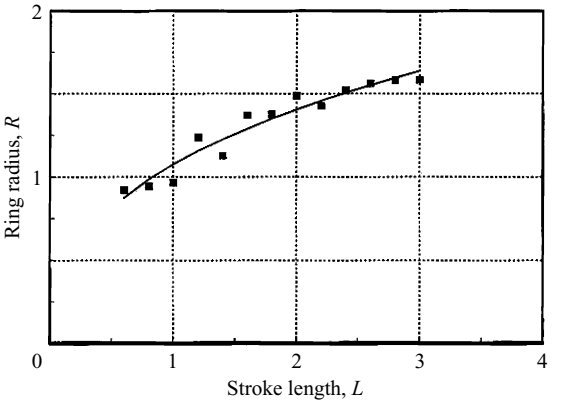

FIGURE 5. Relationship between the observed ring radius R and the piston stroke L. The solid line is given by (2.4): $R = 1.27L^{1/3} - 0.195$. Errors in the measurement are about $\pm 5\,\%$ and increase considerably at short stroke lengths.

a possible logarithmic dependence on time, the bubble radius should also remain constant. Photographs show that the bubble radius is not observably changing size during flight and a sample data set is shown in table 3.

Our model of § 2.1 suggests that vortex ring radii are not necessarily given by the diameter of the gun D_0, but may be both smaller and larger depending on the stroke length. The data shown in figure 5 were taken photographically. We measured the eccentricity of the bubble to be $\gamma = 0.60$. The intercept -0.195 seen in the data in figure 5 arises because arbitrarily small rings cannot be produced, since they are sucked back into the gun. The apparent bubble from the work of Dabiri & Gharib (2004) reproduced in figure 17 below has $\gamma = 0.63$. An image from figure 4 of Didden (1979) has $\gamma = 0.55$.

The discussions of § 2.4 show that for $L = 1.23$ cm and $T = 0.167$ s, the entrainment fraction picked up from ambient fluid after the piston stroke $\eta = (\Omega_b - \Omega_p)/\Omega_b = 0.55$ (see Dabiri & Gharib 2004). Equations (2.4) and (2.17) predict $R = 1.35$ cm and $R_b = 1.76$ cm, compared to measurements 10 cm from the gun which give $R = 1.32 \pm 0.02$ cm and $R_b = 1.79 \pm 0.02$ cm. The experimental value of $R/R_b = 0.74$ is not far from the value 0.77 determined by (2.18), and considerably different from the two-dimensional case of figure 1, where $R/R_b = 0.48$.

Since we really expect the core to grow in time, we can find a rough estimate of the effect on various quantities by amending (2.13), taking account of the total elapsed time by adding the time of flight t to the stroke time T:

$$a = \sqrt{4\nu\,(T + t)}\,. \tag{4.1}$$

	T (s)											
L (cm)	0.05	0.06	0.07	0.08	0.09	0.10	0.11	0.12	0.13	0.14	0.15	0.16
1.0	4.88	4.03	3.70	3.23	2.94	2.59	2.27	1.98	1.82	1.39	1.61	1.47
1.2	6.90	5.26	4.76	4.65	4.03	3.51	2.75	2.45	2.22	2.17	2.00	2.08
1.4	8.20	6.85	6.02	5.75	4.76	4.31	3.40	2.92	2.58	2.43	2.50	2.50
1.6	10.64	8.77	6.85	6.67	5.43	4.85	4.27	3.57	3.07	3.13	2.94	2.78
1.8	12.20	9.90	8.17	7.81	6.58	5.81	5.15	4.50	3.85	3.85	3.68	3.45
2.0	14.97	11.63	10.00	9.26	7.58	6.58	5.88	5.21	4.50	4.39	4.29	3.82
2.2	16.95	13.51	11.90	10.64	8.77	7.46	6.49	5.88	5.95	5.38	4.90	4.46
2.4	19.46	15.29	12.89	11.63	10.00	8.20	7.14	6.41	6.17	5.38	4.90	4.72
2.6	21.46	15.97	14.25	12.72	11.34	9.43	8.59	7.58	6.94	6.17	5.62	5.15
2.8	23.70	18.45	15.06	14.29	11.85	10.20	9.09	8.06	7.58	6.76	6.25	5.95
3.0	26.18	19.84	16.50	15.87	13.16	11.63	9.96	8.77	8.33	7.69	7.04	6.49
3.2	28.90	22.12	18.18	16.67	14.71	12.82	11.11	9.43	8.93	8.33	7.58	7.04

TABLE 4. Ring velocities $V_0\,(\mathrm{cm\,s^{-1}})$ as determined by the methods of § 4.5 as a function of stroke length L (cm) and stroke time T (s).

In particular, the bubble radius R_b given by (2.17) will grow in time if the core size in the the logarithmic factor Λ in (2.10) is replaced by (4.1). Using Kalliroscope as the tracer we took the following data on R_b as a function of the flight time t. T was fixed at 0.5 s, and L at 1.5 cm. We see from table 3 that there is no evidence for growth of R_b. If (4.1) were correct, the bubble radius R_b would have grown by a factor of 1.19 in 12 s.

In order to see whether the bubble was entraining and detraining as predicted by Maxworthy (1972) and observed by Krutzsch (1939), we fired vortex rings through fluid dyed with Baker ink. The fluid was dyed by releasing drops of NaOH into specified locations in the tank. As Krutzsch observed, the inked fluid wrapped up around the outside of the bubble and a little later shed into the wake of the ring. As such it appears that there is a fine balance between the entrainment and detrainment process that suppresses any significant growth of the bubble. The wake behind the bubble was particularly visible in our experiments conducted with Kalliroscope, which highlights regions of vorticity.

4.2. *The velocity of vortex rings*

The simple considerations of § 2.2 are compared to experiment in table 4. The values of V in (2.9) ignore the formation of the rings as they emerge from the gun. We can make an estimate of such values using the methods outlined in § 4.5. The data, fitted to the theoretical function describing slowing, can be extrapolated back to the location of the gun. They are denoted V_0.

The best way to understand these data can be seen from (2.9) written in the form

$$\frac{V}{V_p} = \frac{\gamma \Lambda}{3\pi} \simeq 0.3. \tag{4.2}$$

While there are various slow trends in the data of table 4, the data can be summarized by $V/V_p = 0.328 \pm 0.024$, in good agreement with (4.2). We shall see in § 5.3, however, that this apparent agreement may be accidental.

4.3. *The core size of vortex rings*

We have found that the rotating core can be visualized directly by the Baker technique. What is seen experimentally is shown in figure 6. Figure 6(*a*) shows the

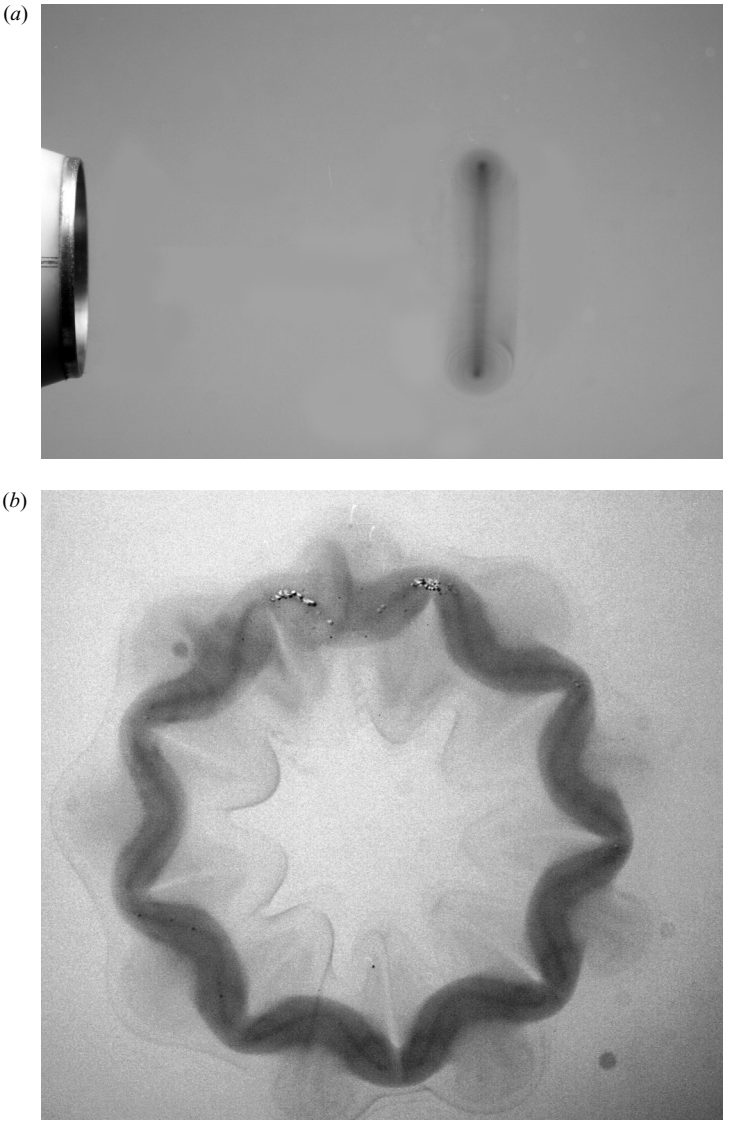

FIGURE 6. Visualization of vortex rings and core. (*a*) Ring and some surrounding flow as seen from above the tank. Here, $L = 1.23$ cm, $T = 0.167$ s. (*b*) Ring as seen looking along the x-axis. Note the thin core and large-amplitude Kelvin waves. A few hydrogen bubbles deliberately introduced help to identify the core. A number of interesting pictures of this instability are contained in Krutzsch (1939).

ring propagating across the tank as seen from above the tank, and figure 6(*b*) shows the ring as seen looking directly into the mouth of the gun. The bending waves in this example are quite evident.

The core size was measured by taking photographs of the ring and measuring the extent of the densest part of the core structure. Results from data with the newer gun are shown in tables 5 and 6. Table 5 shows that the core size scales roughly as the square root of the stroke time, and table 6 shows that the core size is independent of stroke length. The Saffman core radius is $a = \sqrt{4\nu T}$, independent of stroke length.

L (cm)	T (s)	a_{obs} (cm)	a (cm)	a_{obs}/a
2.0	0.05	0.048	0.045	1.07
2.0	0.08	0.053	0.057	0.93
2.0	0.10	0.064	0.063	1.02
2.0	0.12	0.066	0.069	0.96
2.0	0.16	0.073	0.080	0.91

TABLE 5. Core radius as a function of stroke time and stroke length in water ($\nu = 9.78 \times 10^{-3}$ cm^2 s^{-1}) for a constant stroke length. Data taken with the new gun.

L (cm)	T (s)	a_{obs} (cm)	a (cm)	a_{obs}/a
1.4	0.10	0.061	0.063	0.97
1.8	0.10	0.066	0.063	1.05
2.0	0.10	0.064	0.063	1.02
2.2	0.10	0.070	0.063	1.11
2.6	0.10	0.064	0.063	1.02

TABLE 6. Core radius as a function of stroke time and stroke length in water for a constant stroke time. Data taken with the new gun.

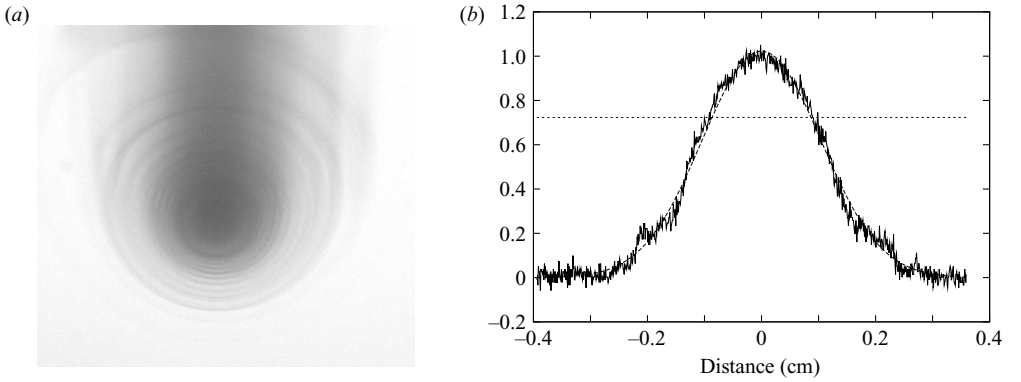

FIGURE 7. (*a*) Photograph of a vortex ring core using a stroke time $T = 0.176$ s. (*b*) Plot of the normalized intensity profile through the middle of the core in (*a*). The half-width at half-power is 0.087 cm. The Saffman core size is 0.082 cm. —, dataset; - - -, Gaussianfit; . . . , half-power.

The results of tables 5 and 6 show that the experimentally determined core size scales directly with the Saffman core size. A set of experiments conducted in a water–glycerol mixture show that the core size scales correctly with kinematic viscosity. However, the results in water–glycerol solutions are not as accurate as in pure water and are not shown here.

If the ring is travelling slowly enough, we can obtain an entire array of intensities such as we show in figure 7(*b*). We have made a fit to this data with a Gaussian whose half-width at half-power is 0.087 cm, in good agreement with the Saffman result. However, we do not know the quantitative relation between vorticity and intensity, so we cannot comment on the distribution of vorticity in the core. We could try to modify the Saffman core diameter from experiment, but to little avail. A 30 % change in a results in only a 6 % change in velocity because the core size is in the logarithmic

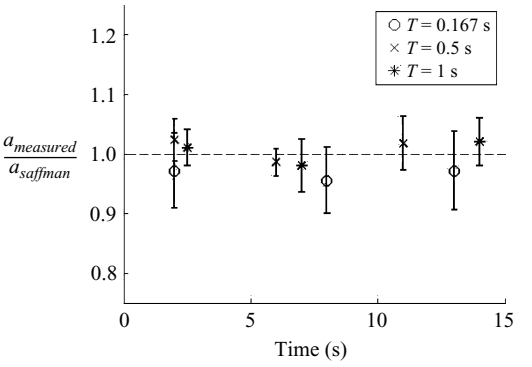

FIGURE 8. The radius of the core as a function of time for several stroke times. Kalliroscope was used for visualization.

term. This is really beyond our current level of measurement ability and so it seems best to adopt Saffman's result as stated by him.

Given the success of the Saffman core model, it would seem natural to believe that the core would grow as the ring propagates across the tank. If the core were growing with time according to (4.1), a slow ring would attain a core radius of several millimetres. The Baker method can only be used to visualize the initial core and not any subsequent growth, because the Baker 'ink' diffuses 6000 times more slowly than vorticity (Mazo *et al.* 2008).

We have attempted to measure the core size of a vortex ring in flight by turning off the electrode in the gun so that the core is not initially marked and sending the ring through a cloud of dark fluid created by injecting a small amount of NaOH in the path of the ring using a syringe. This method was excellent for marking the vortex bubble, but did not mark the core at all. This shows that the vortex bubble seals the interior from oncoming flow, and the fluid inside the bubble is isolated from the rest of the bath.

Since the Baker technique cannot be used to measure the growth of the core, we turned our attention to Kalliroscope, which is useful here because it is distributed throughout the entire tank and does not rely on diffusion to mark the core. The Kalliroscope flakes in the core orient themselves so as to reflect light more intensely in regions of vorticity. If the core grows by diffusion, the Kalliroscope flakes will reorient to mark the new pattern of the core. We see from the data contained in figure 8 that there is no evidence for enlargement of the core. If the core grew as in (4.1), it would have enlarged by a factor of 5.

We observed that the intensity of light reflected from the core decreases over time and while, to our knowledge, no direct correlation between the vorticity and light intensity is possible, it does suggest a loss of circulation within the core as would be expected from a slowing ring.

4.4. *The slowing of vortex rings*

We now turn to measurements of the slowing of vortex rings, and comparison to our model of § 2.5. We use a high-speed camera to track individual vortex rings as they propagate across the tank. The entries in table 4, then, are measurements on a single vortex ring and the value of V_0 comes from the best fit to the propagation data.

Figure 9 shows data taken on the arrival time of rings as a function of distance X from the gun. The solid line is the best fit of (2.26) to the data. This yields a value

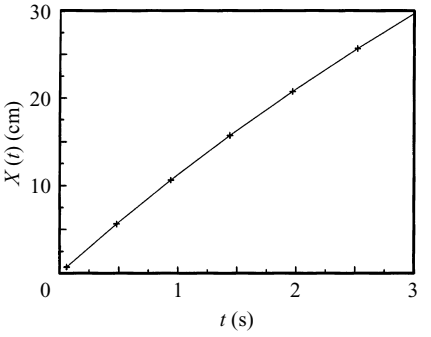

FIGURE 9. Ring distance travelled X as a function of time. Time is measured from the end of the stroke which is 9.5×10^{-3} cm long, and is accomplished in 60 ms.

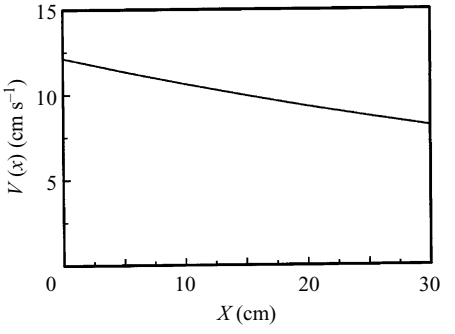

FIGURE 10. Slowing curve as a function of distance calculated from (2.22).

of V_0 of 12 cm s^{-1}, which is a fictitious initial velocity, as it ignores the formation process which extends about one diameter from the mouth of the gun. We generally compare our experimental values of V_0 to the V calculated from (2.9). The data in figure 9 yield the value of the damping coefficient $c = 133$ cm^{-1} defined in (2.25), which together with (2.23) yields the slowing curve of figure 10. The drag coefficient on the core C_{dc} is obtained from (2.25).

The decay of velocity as exponential in distance was first reported by Maxworthy (1972). The decay law t^{-1} quoted by Maxworthy is true only at long times when $t \gg 1$.

Since we really expect the core to grow in time, we can find a rough estimate of the effect of core diffusion upon velocity by combining (2.9) and (4.1), assuming R and Γ are fixed. The result is shown by the dashed curve in figure 11, where we observe that the shape of the decay is dramatically different from experiment. This supports our result that the slowing of thin core rings as a function of time in water occurs because the circulation is decreasing according to (2.22).

Assuming that our drag model captures the dominant factors in slowing the rings, it is useful to deduce the drag coefficient from our experiments. The drag coefficients are calculated as a best fit to the trajectory of the vortex rings obtained with the high-speed camera using (2.23). The results are shown in figure 12, where we call the core drag coefficient C_{dc} to distinguish it from the standard drag on a solid cylinder, which we denote by C_d. Two sets of data are shown, one for the old gun design and one for the new. Note that the values of C_{dc} as shown here are for the drag on the core as envisaged by Saffman. They do drop with Reynolds number, as expected.

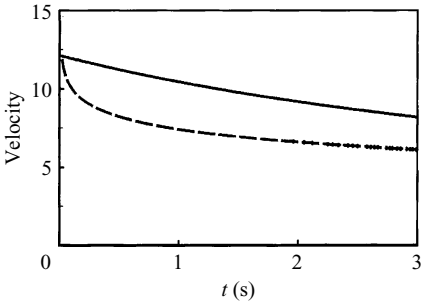

FIGURE 11. The upper curve is the slowing curve measured as described above. The lower curve is obtained by neglecting the drag on the core and assuming the core continues to grow according to (4.1).

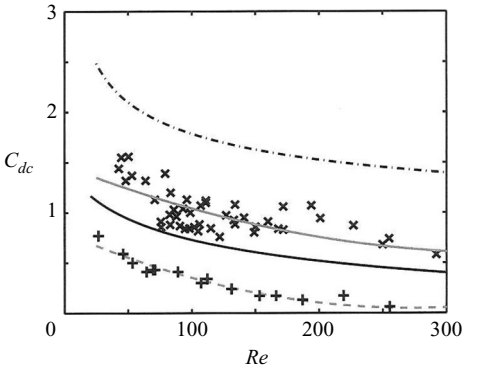

FIGURE 12. The drag coefficient on the core C_{dc} as a function of Reynolds number ($Re = V_0 2a/\nu$). The upper curve is the drag coefficient C_d for a solid cylinder. The solid dark curve represents the drag on an equivalent sphere with radius of the bubble. $\times$, the measured drag coefficients with the old vortex ring gun; grey curve is the best fit given by (4.4). $+$, the drag coefficients measured with the new gun; the lower curve is the best fit to these data given by (4.4).

The first thing worth noting is that the drag coefficients for the new gun are significantly smaller than those measured with the old one. Additionally, the scatter of data for the old gun is much greater than that with the old gun. One possible reason for these differences is that the rings produced by the old gun form Kelvin waves, such as those depicted in figure 6(*b*), at early stages, which cause slowing of the ring. See Barenghi *et al.* (2006) for an analytical discussion of this slowing. The reason we include this data is to illustrate how significant the slowing effect of the waves is relative to other slowing mechanisms, a phenomenon first observed by Krutzsch (1939). We hope to pursue the finer details of this observation in a future study. Additional effects such as the piston velocity as a function of time and generator geometry can also affect this.

For both guns the values of C_{dc} are lower than those for a solid cylinder. While the drag on a rotating solid cylinder can be lower than on a non-rotating cylinder (Goldstein 1938), there is not much precedent for the data shown in figure 12. It is important to note though, that the drag mechanism we are capturing here is quite different from that of a solid rotating cylinder as there are many complex processes that contribute to the drag on the ring that do not exist in the solid cylinder case. For

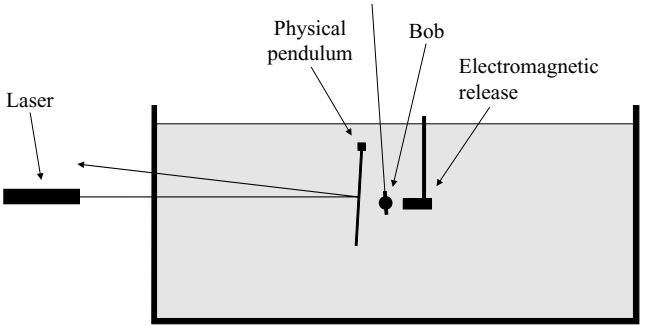

FIGURE 13. Use of a bob pendulum to calibrate the physical pendulum. The bob is suspended by a long string to give it a long period. The bob is drawn back by means of an electromagnet and released to hit the physical pendulum at the bottom of its swing. The velocity of the pendulum at impact is obtained from the measurement in figure 14. The momentum given to the pendulum is then the product of the mass and velocity of the bob.

the sake of comparison, we also include the drag coefficient for a sphere of radius equal to that of the bubble. While the general trend of this coefficient behaves the same for the solid sphere, note that this coefficient is higher than that which we measured with the new vortex ring gun, whereas it is less than that observed with the old gun.

The data from figure 12 can be represented for the range $40 < Re < 300$ by

$$C_{dc} = 7.07 \times 10^{-6} Re^2 - 4.9 \times 10^{-3} Re + 1.49, \tag{4.3}$$

$$C_{dc} = 1.007 \times 10^{-5} Re^2 - 5.52 \times 10^{-3} Re + 0.8, \tag{4.4}$$

which are fits to the data.

We know experimentally that vortex rings in superfluid helium do not experience any dissipation below about 300 mK (Rayfield & Reif 1964). The representation of data from experiments in water in a form such as we show figure 12, implies that viscosity is the origin of the drag. In order to test this, we carried out the following experiment. We measured the drag coefficient with stroke $L = 2.0$ cm, $T = 0.33$ s and obtained $C_{dc} = 0.52$ in water at $Re = 43.9$. We then prepared a glycerol–water solution of kinematic viscosity $\nu = 1.7 \times 10^{-2}$ cm^2 s^{-1} and repeated the measurement obtaining $C_{dc} = 0.60$ at a Reynolds number of 33.3. Equation (4.4) gives a drag coefficient $C_{dc} = 0.52$ at $Re = 43.9$, and $C_{dc} = 0.63$ at $Re = 33.3$. These results, well within the observed scatter, confirm that the effect of viscosity on drag coefficient is properly accounted for by Reynolds-number scaling.

4.5. *Measurement of the impulse of vortex rings*

A familiar measure of impulse is the 'ballistic pendulum' consisting of a bag of sand suspended by a rope which was used in tests of bullets before modern electronics was developed. A bullet fired into the bag causes the bag to swing, and hence gives a measure of the impulse imparted by the bullet. In our case, we decided to make a physical pendulum of 6 in $\times$ 6 in aluminium plate 1/32 in thick. Tests showed that this is large enough to collect all the momentum from a vortex ring approximately 1 in in diameter. The problem, then, was to find a way to calibrate this pendulum which is completely submerged in water without trying to understand effects such as viscosity and added mass of such an awkward object. The method adopted is shown in figures 13, 14 and 15. The key idea was to calibrate the pendulum by means of a

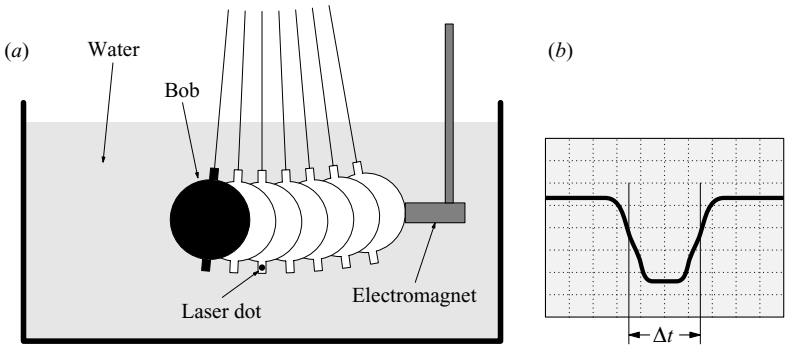

FIGURE 14. The speed of the bob at its lowest point is measured as shown in (*a*). The bob is released and a small rod on its bottom occults the laser at its lowest point of trajectory which results in an oscilloscope trace similar to (*b*). Since the laser beam is roughly the same size as the rod on the bob there are diffraction effects and a separate calibration must be used to find its apparent diameter. Using different initial displaments of the bob, we can calculate the impulse given to the pendulum as a function of the angle of deflection of the physical pendulum.

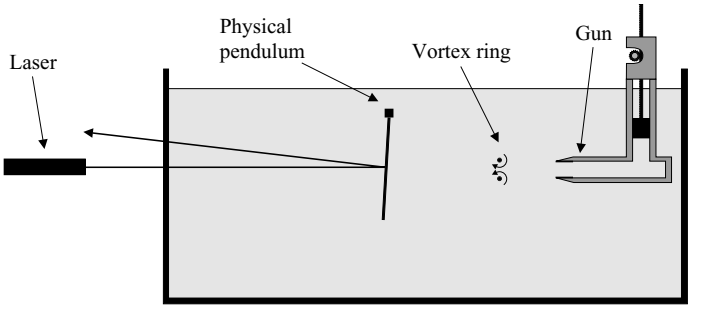

FIGURE 15. The last step is to remove the bob pendulum and fire vortex rings at the physical pendulum. The original gun was used in these experiments. Since we have an absolute calibration of the deflection as a function of momentum, we can determine the impulese of the vortex ring without knowing anything about the physical characteristics of the pendulum.

bob pendulum suspended above the tank on a long string. The bob had a short rod attached to its bottom for timing purposes. Measurements were taken when the bob reached its lowest point.

Angular deflections were measured using a laser beam hitting a small mirror on the rear of the physical pendulum and read on a metre stick some distance away. In a more recent revision of the apparatus, we used a solid-state laser diode and lens as a source of light and a line scan CCD angle sensor, outputting to an oscilloscope. This gave a reliable measure of deflection which can be difficult to do by eye when the deflections are very rapid.

The momentum calibration was expressed as a second-order power series in the angle of deflection of the pendulum. Thus, measurement of the deflection of the pendulum gave the experimental value of impulse P_e. It is not entirely clear to us what role the added mass plays in this calibration. If it does apply, the added mass is 1.84 g compared to the physical mass of the bob which is 28.8 g. The values of P_e in tables 7 and 8 would increase by 6.4 %.

L (cm)	1.5	2.0	2.5	3.0	3.0	3.0
T (s)	0.05	0.05	0.05	0.05	0.075	0.10
V (cm s^{-1})	9.4	15	20.5	26.2	16.2	11.6
R (cm)	1.37	1.55	1.65	1.70	1.70	1.70
$a \times 10^2$ (cm)	4.47	4.47	4.47	4.47	5.48	6.33
$P_e \times 10^3$ (g cm s^{-1})	257	448	632	877	622	468
$P_v \times 10^3$ (g cm s^{-1})	193	432	714	978	629	464
P_e/P_v	1.3	1.0	0.88	0.89	0.98	1.0

TABLE 7. Measured impulse P_e for vortex rings from a gun with $D_0 = 2.54$ cm compared to impulse P_v calculated from velocity measurements, (2.9).

L (cm)	1.5	2.0	2.5	3.0	3.0	3.0
T (s)	0.05	0.05	0.05	0.05	0.075	0.10
$P_e \times 10^3$ (g cm s^{-1})	257	448	632	877	622	468
$P_p \times 10^3$ (g cm s^{-1})	228	405	633	912	608	456
P_e/P_p	1.1	1.1	1.0	0.96	1.0	1.0

TABLE 8. Comparison between the measure impulse P_e and the momentum given to the water by the piston, P_p.

We can compare the momentum to other measurements by using the circulation Γ_v as calculated from the velocity as described in § 2.2, equation (2.9). Then, $P_v = \rho\pi R^2 \Gamma_v$.

Table 7 shows the results of six different calibration trials with various stroke lengths L and stroke times T. We see that the direct measurement of impulse P_e is in good agreement with the impulse calculated from velocity measurements.

The mass displaced by the piston $M_p = \rho\pi R_0^2 L$ and the momentum given to the water by the piston in the gun is

$$P_p = M_p V_p. \tag{4.5}$$

We show in table 8 a comparison between the measured impulse P_e and P_p.

4.6. *The energy of vortex rings*

Since the expression for the velocity of a viscous ring (2.9) is not much different from the corresponding inviscid result (1.6), we might hope that the energy might not be too far from the inviscid result

$$E = \tfrac{1}{2}\rho\Gamma^2 R\left[\ln\frac{8R}{a} - \alpha\right] = \tfrac{1}{2}\rho\Gamma^2 R\Lambda'. \tag{4.6}$$

The energy given to the water in the gun by the piston is called E_p,

$$E_p = \tfrac{1}{2}M_p V_p^2 = \frac{P_p^2}{2M_p}. \tag{4.7}$$

However, there are a couple of subtle points required in order to show this. The first is the added mass discussed in § 2.4. The mass of water travelling with the bubble, corrected for added mass, is $M_b = \Omega_b\rho(1+k)$ and the momentum of water travelling with the bubble is $P_b = M_b V$. The kinetic energy associated with the travelling bubble is $P_b^2/2M_b$. Now we have shown experimentally that $P_p = P_b$, and that $M_b > M_p$. Thus, the kinetic energy associated with the bubble is considerably less than E_p. The

Γ_{obs} (cm^2 s^{-1})	11.4	16.6	21.9	27.0	31.0
Γ_{calc} (cm^2 s^{-1})	10.5	12.3	13.8	15.0	16.0
$\Gamma_{obs}/\Gamma_{calc}$	1.09	1.35	1.59	1.80	1.90

TABLE 9. Comparison of circulation measured by Didden (1979) with our calculated values. Reynolds numbers here are about $100\,\Gamma$.

difference must be some potential energy associated with the bubble. It is known that rectilinear vortices have an energy per unit length, or tension (see Donnelly 1991, p. 13). Thus the ring has, in effect, an energy per unit length multiplied by $2\pi R$ and that will be the energy E of the ring (4.6).

Let us explore this numerically. For a typical ring with $L = 1.23$ cm, $T = 0.167$ s, we find $P_p^2/2M_p = 169.0$ and $P_b^2/2M_b = 46.58$. The difference is given by (4.6) with $\alpha = 2.04$, not far from the values in table 1.

5. Comparison with the work of other investigators

We have not located another study of vortex rings with such thin cores. Nevertheless, it is useful to compare our formulae to certain other experimental situations. Most previous studies have focused on larger stroke time T and larger formation times, L/D. Nevertheless, we compare our formulae to other experimental studies.

Two of the most influential papers in this field were written by Maxworthy (1972, 1974). His studies were carried out on a somewhat different orifice geometry and initiated by a hand-operated syringe, involved thick core rings, making it difficult to compare his results with ours. A careful discussion of Maxworthy's work is contained in Dabiri & Gharib (2004).

We noted the comparison between our measurements of eccentricity γ and those of other authors in § 4.1.

5.1. *The radius of vortex rings*

We discussed in § 4.1 measurements of ring radii and a formula (2.4) for estimating their radius. Auerbach (1988) reports

$$\frac{R}{R_0} = 0.937 \left(\frac{L}{R_0}\right)^{1/3}, \quad 0.6 \leqslant \frac{L}{R_0} \leqslant 2. \tag{5.1}$$

Our result can be written

$$\frac{R}{R_0} = 1.03 \left(\frac{L}{R_0}\right)^{1/3}, \quad 0.4 \leqslant \frac{L}{R_0} \leqslant 2.4, \tag{5.2}$$

which is in good agreement with Auerbach's result.

5.2. *Vortex circulation*

Didden (1979) reports measurements of ring circulation with a 5 cm diameter tube and a piston velocity of 4.6 cm s^{-1} taken at 15 cm from the gun. We show in table 9 the comparison between Didden's measurements of circulation reported in figure 17 of his paper, and our calculations based on (2.8) and Didden's experimental conditions.

After our impulse measurements were completed, we found that a related measurement of impulse by means of a surge tube was carried out by Baird *et al.* (1977). Although their method is less accurate, they too verified that the momentum of the vortex ring is just equal to the momentum imparted by the piston.

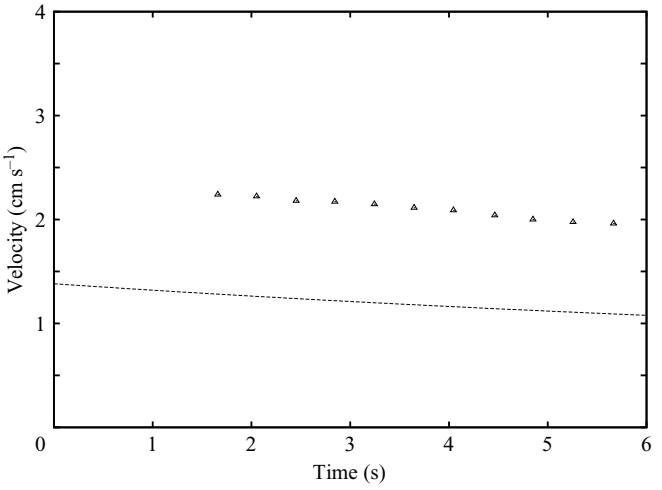

FIGURE 16. Comparison of our decay model with the measurements of Dabiri & Gharib (2004) for the case $L/D = 2$. The upper symbols are the experimental data, the line represents 2.24.

5.3. *Vortex velocities*

Baird *et al.* (1977) showed that the ring velocity is approximately equal to 0.5 Vp. That proportionality is demonstrated in our (2.9). It can be seen that our formulae give a surprisingly good account of their data especially for smaller values of L/D_0. These are very fast rings with sometimes large formation times. Their figure 5 shows a bubble with $\gamma = 0.55$, in reasonable agreement with our value of 0.60.

Gharib *et al.* (1998) have made systematic measurements of vortex circulations as a function of L/D ratios. Their results show that the flow for large L/D consists of a leading vortex ring followed by a trailing jet. Clearly, our model does not contain such information, but the results show that our model gives reasonable results for small L/D, say $L/D < 2$.

Our model predicts (4.2) based on Saffman's value of $\beta = 0.558$. Our data is in fair agreement with (4.2): $V/V_p = 0.328 \pm 0.024$. However, our new gun gives $V/V_p = 0.63$, Baird *et al.* (1977) give $V/V_p = 0.493 \pm 0.072$ and Dabiri & Gharib (2004) give $V/V_p = 0.4$. At first sight there is nothing we can do to alter (4.2). However, we can appeal again to Saffman (1978) who shows that for viscous vortex rings the quantity β, and hence the speed of rings, can depend upon the distribution of vorticity in the core, see his equations (2.17), (3.5) and (3.6). Indeed, the core structure itself affects the ring velocity as we see in § 1.1. This problem clearly deserves further investigation. In the meantime, we suggest taking the ratio V/V_p as a figure of merit for each gun design.

5.4. *The slowing of vortex rings and decay of circulation*

Dabiri & Gharib (2004) have studied the decay of both velocity and circulation for vortex rings fired at a piston velocity of 5.5 cm s^{-1} from a 2.54 cm diameter gun. Using digital particle-image velocimetry (DPIV), the authors measured the decay of ring velocity and circulation as a function of time. We digitized their results for velocity in their figure 7(a) and circulation in figure 9 for the case of zero counterflow. Figure 16 shows the decay of velocity as a function of time according to (2.24). Both the decay of velocity and decay of vorticity were captured well by our methods. The magnitude

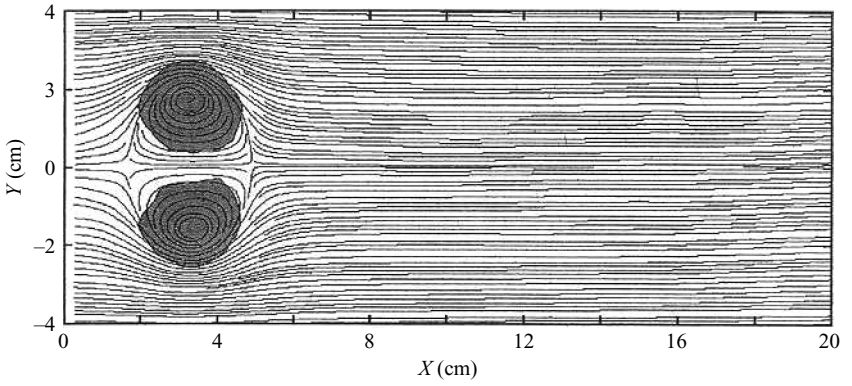

FIGURE 17. Instantaneous streamlines and vorticity patches for $L/D = 2$ and $T = 1.67$ s. (After Dabiri & Gharib 2004.)

of the velocity itself depends on the structure of the gun, as discussed in the previous section.

Our model predicts that the rate of decay if circulation is proportional to the slowing of the ring (2.22):

$$\frac{\mathrm{d}\Gamma}{\mathrm{d}t} = \frac{4\pi R}{\Lambda}\frac{\mathrm{d}V}{\mathrm{d}t}. \tag{5.3}$$

Approximating the velocity and circulation decay by straight lines over their limited range, we find, very roughly $\mathrm{d}V/\mathrm{d}t = -0.074$, and $\mathrm{d}\Gamma/\mathrm{d}t = -0.456$. The ratio of these quantities is 6.16, not far from $4\pi R/\Lambda = 6.92$.

While we find fair agreement on the value of the velocity for the case of figure 16, our core size is calculated to be $a = 0.192$ cm at the end of the stroke (0.924 s). Figure 17 shows a core at 1.67 s nearly filling the bubble. The darker shaded region corresponds to regions of vorticity greater than $1\,\mathrm{s}^{-1}$.

Dabiri & Gharib (2004) show in their figure 6, peak vorticities of order $10\,\mathrm{s}^{-1}$. Using our core size, we find peak vorticities about an order of magnitude greater. This is probably due to the finite resolution of the PIV instrument used by them, which has a pixel resolution of approximately $0.19 \times 0.19\,\mathrm{mm}^2$ and laser time pulse of 18 ms.

Shusser & Gharib (2000) recommended a formula for the velocity of thick rings based on the slug model (equation (23) of their paper),

$$V_{sg} = 0.5352\sqrt{\frac{\rho\Gamma^3}{\pi P}}. \tag{5.4}$$

Applying (5.4) using their expressions for Γ and P to the data in figure 17, we find the velocity $V = 1.2\,\mathrm{cm\,s}^{-1}$ very close to our result shown there. In the notation of this paper

$$V_{sg} = 0.5352\frac{\Gamma_s}{\pi R_0}. \tag{5.5}$$

The principal difference between (5.4) and (2.9) is to replace our logarithmic term by a constant and the ring radius by the orifice radius.

Weigand & Gharib (1997) studied the evolution of laminar vortex rings using laser-Doppler anemometry (LDA) and DPIV methods and present a discussion on the slowing of vortex rings. They consider the analysis of Saffman (1970) for rings

without small core sizes, which is based on dimensional arguments. This argument states that rings slow owing to loss of impulse due to an increase in the vortex ring radius, R, and it is argued that the velocity decays as

$$V \approx \frac{1}{k}(R^2 + k'\nu t)^{-2/3}, \tag{5.6}$$

where k and k' are constants. Fitting these constants, they find reasonable agreement between experimental measurements and predictions of the ring velocities. However, as discussed in § 4.1, and table 2, we found that the radius of the ring did not increase during flight, and therefore (5.6) does not seem to apply to our experiments.

Fukumoto & Moffatt (2000) have considered the motion of a vortex ring in a viscous fluid starting from an infinitely thin circular loop of radius R at time $t = 0$. They have carried Saffman's formula (2.12) a further step.

$$V = \frac{\Gamma}{4\pi R}\left\{\ln\frac{4R}{\sqrt{\nu t}} - 0.558 - 3.6716\frac{\nu t}{R^2}\right\}. \tag{5.7}$$

Equation (5.7) describes slowing of vortex rings. It is in good agreement with direct numerical simulations by Stanaway, Cantwell & Spalart (1988) and on a scale such as we show in the lower curve of figure 11, it is very close to the Saffman result shown there.

6. Conclusions and discussion

The expressions developed in this paper are in many ways a matter of guessing, and we may have strayed too far from the real physics of the situation. Nevertheless, it is clear that these results correlate with a substantial amount of the published data, especially that of recent years. The situation on several fronts remains unsatisfactory. It is difficult to try to imagine why the vortex core does not diffuse. Our picture does not contain any information about rings of formation time L/D greater than 4.

We summarize the relations developed in this paper below, for convenience.

$L,\ T$	stroke length and stroke time,
$V_p = L/T$	mean velocity of the piston,
$L/D_0 = V_pT/D_0$	dimensionless formation time,
$L/D_0 = 4$	formation number,
$D_0,\ R_0$	diameter and radius of the gun,
ν	kinematic viscosity of the fluid,
γ	eccentricity of the bubble,
k	Bessel added mass factor,
C_{dc}	measured drag coefficient on a ring.

Saffman velocity for propagation of a vortex ring in a viscous fluid

$$V = \frac{\Gamma}{4\pi R}\Lambda, \tag{6.1}$$

$$\Lambda = \ln\left(\frac{8R}{a}\right) - \beta, \tag{6.2}$$

$$\beta = 0.558. \tag{6.3}$$

Saffman core size

$$a = \sqrt{4\nu T}. \tag{6.4}$$

Radius of the vortex ring

$$R = \sqrt[3]{\frac{3R_0^2 L}{4\gamma}}. \tag{6.5}$$

Circulation of the vortex ring

$$\Gamma = \frac{R_0^2 L V_p}{R^2} = \frac{R_0^2 L^2}{R^2 T}. \tag{6.6}$$

Velocity of the ring at formation

$$V_0 = \frac{\Gamma}{4\pi R}\left(\ln\frac{8R}{a} - 0.558\right) = \frac{\gamma V_p}{3\pi}\Lambda. \tag{6.7}$$

Radius of the bubble

$$R_b = \sqrt[3]{\frac{9\pi R_0^2 L}{4\gamma^2 \Lambda\,(1+k)}}. \tag{6.8}$$

Entrained fraction of fluid in the bubble

$$\eta = 1 - \frac{\Lambda\,(1+k)\,\gamma}{3\pi}. \tag{6.9}$$

Velocity of the ring as a function of distance

$$V = V_0 \mathrm{e}^{-cX}. \tag{6.10}$$

Velocity of the ring as a function of time

$$V = \frac{V_0}{(1 + V_0 ct)}. \tag{6.11}$$

Distance travelled by the ring in time t

$$X(t) = \frac{1}{c}\ln\left(V_0 ct + 1\right). \tag{6.12}$$

Damping coefficient of vortex ring velocity

$$c = \frac{C_{dc} a \Lambda}{2\pi R^2}. \tag{6.13}$$

Energy of a ring at formation

$$E = \tfrac{1}{2}\rho \Gamma^2 R \Lambda', \tag{6.14}$$

$$\Lambda' = \ln\left(\frac{8R}{a}\right) - \alpha, \tag{6.15}$$

$$\alpha = 2.05. \tag{6.16}$$

We are grateful to many colleagues who have given advice and assistance in this investigation. They include John Dabiri, Morteza Gharib,Tony Leonard, Tim Nickels, Renzo Ricca, Karim Shariff and Joe Vinen.

This research was supported by the US National Science Foundation under grants DMR 9529609 and DMR 0202554.

REFERENCES

Auerbach, D. 1988 Some open questions on the flow of circular vortex rings. *Fluid Dyn. Res.* **2**, 209–213.

Baird, M. H. I., Wairegi, T. & Loo, H. J. 1977 Velocity and momentum of vortex rings in relation to formation parameters. *Can. J. Chem. Engng* **55**, 19–26.

Baker, D. J. 1966 A technique for the precise measurement of small fluid velocities. *J. Fluid Mech.* **26**, 573–575.

Barenghi, C. F., Donnelly, R. J. & Vinen, W. F. 1983 Friction on quantized vortices in helium II. *J. Low Temp. Phys.* **52**, 189–247.

Barenghi, C. F., Hänninen, R. & Tsubota, M. 2006 Anomalous translational velocity of a vortex ring with finite-amplitude Kelvin waves. *Phys. Rev.* E **74**, 046303.

Dabiri, J. O. & Gharib, M. 2004 Fluid entrainment by isolated vortex rings. *J. Fluid Mech.* **511**, 311–331.

Didden, N. 1979 On the formation of vortex rings: rolling-up and production of circulation. *J. Appl. Maths Phys.* **30**, 101–116.

Donnelly, R. J. 1991 *Quantized Vortices in Helium II*. Cambridge University Press.

Fetter, A. L. & Donnelly, R. J. 1966 On the equivalence of vortices and current filaments. *Phys. Fluids* **9**, 619–620.

Fraenkel, L. E. 1972 Examples of steady vortex rings of small cross-section in an ideal fluid. *J. Fluid Mech.* **51**, 119–135.

Fukumoto, Y. & Moffatt, H. K. 2000 Motion and expansion of a viscous vortex ring. *J. Fluid Mech.* **417**, 1–45.

Gauthier, G., Gondoret, P. & Rabaud, M. 1998 Motion of anisotropic particles: application to visualization of three dimensional flows. *Phys. Fluids* **10**, 2147–2154.

Gharib, M., Rambod, E. & Shariff, K. 1998 A universal time scale for vortex ring formation. *J. Fluid Mech.* **360**, 121–140.

Goldstein, S. 1938 *Modern Developments in Fluid Dynamics*, vols. 1 and 2. Oxford University Press.

Hollerbach, R., Wiener, R. J., Sullivan, I. S. & Donnelly, R. J. 2002 The flow about a torsionally oscillating sphere. *Phys. Fluids* **14**, 4192–4205.

Kiknadze, L. & Mamaladze, Y. 2002 The waves on the vortex ring in H II. *J. Low Temp. Phys.* **126**, 321–326.

Krueger, P. S. 2005 An over-pressure correction to the slug model for vortex ring circulation. *J. Fluid Mech.* **545**, 427–443.

Krutzsch, C. H. 1939 Uber eine experimentell beobachtete erscheinung an wirbelringen bei ihrer translatorischen bewegung in wirklichen flussigkeiten. *Annln Phys.* **35**, 497–523.

Lamb, H. 1945 *Hydrodynamics*. Dover.

Lim, T. T. & Nickels, T. B. 1995 Vortex rings. In *Fluid Vortices* (ed. S. I. Green). Kluwer.

Loitsyanskii, L. G. 1966 *Mechanics of Liquids and Gases*. Pergamon.

Matisse, P. & Gorman, M. 1984 Neutrally bouyant anisotropic particles for flow visualization. *Phys. Fluids* **27**, 759–760.

Maxworthy, T. 1972 The structure and stability of vortex rings. *J. Fluid Mech.* **51**, 15–32.

Maxworthy, T. 1974 Turbulent vortex rings. *J. Fluid Mech.* **64**, 227–239.

Mazo, R. M., Hershberger, R. E. & Donnelly, R. J. 2008 Observations of flow patterns by electrochemical means. *Exps. Fluids* **44**, 49–57.

Park, K., Barenghi, C. F. & Donnelly, R. J. 1980 Subharmonic destabilization of Taylor vortices near an oscillating cylinder. *Phys. Lett.* **78**A, 152–154.

Rayfield, G. & Reif, F. 1964 Quantized vortex rings in superfluid helium. *Phys. Rev.* **136**, A1194–1208.

Reynolds, O. 1876 On the resistance encountered by vortex rings, and the relation between the vortex rings and streamlines of a disk. *Nature* **14**, 477–579.

Roberts, P. H. & Donnelly, R. J. 1970 Dynamics of vortex rings. *Phys. Lett.* **31**A, 137–138.

Roberts, P. H. & Grant, J. 1971 Motions in a bose condensate I. the structure of the large circular vortex. *J. Phys.* A**4**, 55–72.

Rogers, W. B. 1858 On the formation of rotating rings by air and liquids under certain conditions of discharge. *Am. J. Sci.* (ser. 2) **26**, 246–268.

Saffman, P. G. 1970 The velocity of viscous vortex rings. *Stud. Appl. Maths.* **49**, 371–380.

Saffman, P. G. 1978 The number of waves on unstable vortex rings. *J. Fluid Mech.* **84**, 625–639.

Saffman, P. G. 1981 Dynamics of vorticity. *J. Fluid Mech.* **106**, 49–58.

Savas, O. 1985 On flow visualization using reflective flakes. *J. Fluid Mech.* **152**, 235–248.

Scase, M. M. & Dalziel, S. B. 2006 An experimental study of the bulk properties of vortex rings translating through a stratified fluid. *Euro. J. Fluid Mech.* **25**, 302–320.

Shariff, K. & Leonard, A. 1992 Vortex rings. *Annu. Rev. Fluid Mech.* **24**, 235–279.

Shusser, M. & Gharib, M. 2000 Energe and velocity of a forming vortex ring. *Phys. Fluids* **12**, 618–621.

Stanaway, S. K., Cantwell, B. J. & Spalart, P. R. 1988 Navier–Stokes simulations of axisymmetric vortex rings. In *AIAA 26th Aerospace Sciences Meeting, Reno, Nevada* pp. 1–14.

Weigand, A. & Gharib, M. 1997 On the evolution of laminar vortex rings. *Exps. Fluids* **22**, 447–457.